Acta Medica
Okayama

Original Article

In Vitro Assessment of Factors Affecting the Apparent Diffusion Coefficient of Ramos Cells Using Bio-phantoms

Takanori Sasaki[a], Masahiro Kuroda[b]*, Kazunori Katashima[c], Masakazu Ashida[c],
Hidenobu Matsuzaki[c], Junichi Asaumi[c], Jun Murakami[c], Seiichiro Ohno[d],
Hirokazu Kato[b], and Susumu Kanazawa[a]

Departments of [a]Radiology, [c]Oral and Maxillofacial Radiology, Okayama University Graduate School of Medicine,
Dentistry and Pharmaceutical Sciences, [b]Radiological Technology, Graduate School of Health Sciences, Okayama University, and
[d]Central Division of Radiology, Okayama University Hospital, Okayama 700–8558, Japan

The roles of cell density, extracellular space, intracellular factors, and apoptosis induced by the molecularly targeted drug rituximab on the apparent diffusion coefficient (ADC) values were investigated using bio-phantoms. In these bio-phantoms, Ramos cells (a human Burkitt's lymphoma cell line) were encapsulated in gellan gum. The ADC values decreased linearly with the increase in cell density, and declined steeply when the extracellular space became less than 4 μm. The analysis of ADC values after destruction of the cellular membrane by sonication indicated that approximately 65% of the ADC values of normal cells originate from the cell structures made of membranes and that the remaining 35% originate from intracellular components. Microparticles, defined as particles smaller than the normal cells, increased in number after rituximab treatments, migrated to the extracellular space and significantly decreased the ADC values of bio-phantoms during apoptosis. An *in vitro* study using bio-phantoms was conducted to quantitatively clarify the roles of cellular factors and of extracellular space in determining the ADC values yielded by tumor cells and the mechanism by which apoptosis changes those values.

Key words: apparent diffusion coefficient value, cell density, extracellular space, bio-phantom

D iffusion-weighted (DW) imaging of MRI is a useful method for the diagnosis and post-treatment follow-up of tumors [1, 2]. DW imaging enables us to measure the apparent diffusion coefficient (ADC). It is well known that ADC values are lower in tumor tissues and increase after treatment [1, 2]. The ADC values have frequently been used as indicators of the diffusion of water molecules [3]. The presence of barriers with various biophysical properties may affect water diffusivity by hindering Brownian motion. These barriers consist of small intracellular compartments and cell membranes that divide intracellular from extracellular spaces. Moreover, biophysical components, specifically sodium ions, ATPs, lactates, and *N*-acetyl aspartate, also affect the diffusion of water molecules [4, 5].

To investigate the ADC values of intra- and extracellular spaces, we previously developed new bio-phantoms [6] containing gellan gum and living tumor cells, which enable us to place cells uniformly at

arbitrary cell densities in bio-phantoms. Gellan gum does not affect the ADC values of cells being used in bio-phantoms [6], and it has no cytotoxicity [7]. In addition, as cells are enclosed within bio-phantoms at room temperature, cells were not damaged by heat during the production of the bio-phantoms. Using these bio-phantoms, we clarified that the extracellular space plays an important role in determining the ADC values of bio-phantoms [6]. To what degree, however, remains to be answered.

In vivo studies have suggested that the factors visualized by DW imaging in tumor tissues include cell density [8, 9], extracellular spaces [10, 11], intracellular factors such as intracellular components and cell membrane structures [12, 13], and blood flow in the capillary vessels [14]. Because most of these factors were identified by a comparison between in vivo ADC values and histological findings of human [9–12, 15] and animal [8, 13, 14, 16] tissues, it has been difficult to clarify the degree to which each factor contributes to the ADC values. In our in vitro study, we analyzed the factors affecting ADC values using bio-phantoms, with a particular focus on the roles of cell density, extracellular spaces, and intracellular factors. In addition, by means of the destruction of the cell membrane using sonication, the roles of extracellular space and intracellular factors were analyzed.

It has been reported recently that apoptosis occurring due to chemotherapeutic drugs and radiation changed the in vivo ADC values of animal tumors [17–19]. Although several mechanisms underlying the changes in ADC have been posited, including dilatation of the extracellular spaces and the decrease in cell density due to cell shrinkage and cell death, it has not been possible to identify the crucial factors among them. In this in vitro study, the molecularly targeted drug rituximab, which is an anti-CD20 antibody for lymphoma [20], was used to induce apoptosis of Ramos cells [21], a CD20-positive human Burkitt's lymphoma cell line. The alteration of ADC values during apoptosis and the mechanisms underlying the alteration were then investigated.

Materials and Methods

Cells and cell culture.　　Ramos cells, a CD20-positive Burkitt's lymphoma cell line, were kindly provided by the RIKEN Cell Bank (Ibaraki, Japan) and used for the present study. The cells were cultured in RPMI 1640 medium (Gibco, Grand Island, NY, USA) supplemented with 10% fetal bovine serum (Filtron PTY, Brooklyn, Australia) and 1% penicillin-streptomycin-neomycin (Gibco). Cells were cultured in an incubator with 5% CO_2 plus 95% air at 37℃. The rotational culture was performed using spinner flasks on a magnetic stir plate set to 10 or 15 rpm in an incubator (Fig. 1A).

Measurements of the number and the center-to-center distance of cells.　　Cells with diameters larger than 8 μm were counted by an electric cell counter (Coulter Electronics, Luton, UK) before each treatment. The cell density was calculated based on the cell count. The center-to-center distance (2r) between cells was calculated by applying the Kepler conjecture [22]. The Kepler conjecture is a about in three-dimensional Euclidean space. It says that no arrangement of equally sized spheres filling space has a greater average density than that of the cubic close-packing (face-centered cubic) and hexagonal close-packing arrangements. The density of these arrangements is slightly greater than 74%. We assumed that 74% of the volume of a bio-phantom is a cellular volume when the cell density is maximal. We assumed that the cellular volume is shown by $4/3\,\pi r^3$ and calculated r. Then the center-to-center distance (2r) of cells is given by the formula $2r = 1.12\,\rho^{-1/3}$, where ρ indicates the cell density.

Rituximab treatment for the induction of apoptosis.　　The cells were seeded into a spinner flask containing 250 mL medium. After 6 days, rituximab (Chugai Pharmaceutical, Tokyo, Japan) was added into spinner flasks in which cell density was $5.0 - 9.0 \times 10^5$/mL and the cells were cultured in medium with 10 μg/mL rituximab at 37℃ for 24 h. Then the cells were encapsulated in a microcuvette to make bio-phantoms from the cell pellets as described below.

Encapsulation of cells into bio-phantoms.　　The Ramos cells that were not treated and that were treated by sonication to destruct the cell membranes were encapsulated into bio-phantoms (Fig. 1B, C) according to a previously reported method [6]. In brief, the medium containing the cells was concentrated to about 2 mL and then moved into the microcuvette. The medium in the cuvette was centrifuged at, 1500 rpm for 5 min and the supernatant was removed
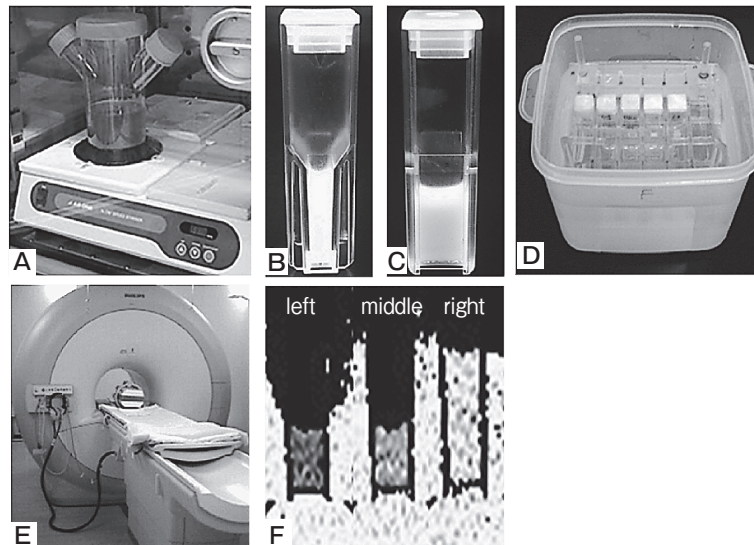
Fig. 1   The phantoms and methods used in this study. (**A**) Rotational culture using a spinner flask in the incubator. (**B**) Front image of a bio-phantom including tumor cells. (**C**) Lateral image of a bio-phantom. (**D**) A phantom container of bio-phantoms. (**E**) MR imaging of bio-phantoms using a 1.5T MRI system. (**F**) ADC map of bio-phantoms that were prepared at 1.0×10^9/mL (left), 5.0×10^8/mL (middle), 3.5×10^7/mL (right).

to make cell pellets in which cell density was between 1.1×10^9/mL and 1.3×10^9/mL. The cell pellets were then diluted by 0. 5 w/w% gellan gum, which had been dissolved in distilled water and highly concentrated ($\times 10$) phosphate-buffered saline (PBS), to yield a final concentration of 0.25 w/w% gellan gum in isotonic ($\times 1$) PBS. Cells were encapsulated in bio-phantoms containing gellan gum so as to achieve a final cell density between 3.0×10^7/mL and 8.0×10^8/mL. To make bio-phantoms in which cell density was between 1.1×10^9/mL and 1.3×10^9/mL, the cell pellets themselves were used as bio-phantoms without using gellan gum. Similarly, to make bio-phantoms using rituximab-treated cells, the cell pellets themselves were used as bio-phantoms without using gellan gum.

Light-microscopice observation and measurement of cell diameter.   The bright-field images of cells were observed by phase-contrast fluorescent microscopy (Olympus, Tokyo, Japan) [23]. Images of 100 cells were analyzed using the image processing software Image-J (National Institutes of Health, Bethesda, MD, USA). The cell diameters were measured with bright-field images in order to calculate the mean $\pm$ standard deviation.

Observation by scanning electron micro-

scope.   Cells were fixed in 2% glutaraldehyde and 2% formaldehyde in PBS and then rinsed, dehydrated in an ethanol series (50–100%), and replaced in t-butyl alcohol. After lyophilization, the specimens were coated with osmium metal. Finally, the specimens were observed by a scanning electron microscope (S–4800, Hitachi High Technologies, Tokyo, Japan) at the Central Research Laboratory, Okayama University Medical School.

Observation by transmission electron microscope.   Cells were fixed in 2.5% glutaraldehyde, then rinsed with PBS, post-fixed in osmium tetroxide, and rinsed again with PBS. The specimens were then dehydrated in an ethanol series (50–100%), treated with propylene oxide, and embedded in epoxy resin. Thin sections were stained with uranyl acetate and lead citrate, and were observed by a transmission electron microscope (H–7650, Hitachi High Technologies) at the same laboratory.

Flow cytometric analysis.   The double-staining method using enhanced green fluorescent protein-labeled Annexin V (AV), and propidium iodide (PI) was used to estimate the number of cells undergoing apoptosis and necrosis as described previously [23]. Briefly, 3×10^5 cells were stained with AV using an Annexin V-EGFP Apoptosis Detection kit (Becton

Dickinson, San Diego, CA, USA) and 0.2 nM PI (Sigma, St. Louis, MO, USA). After staining, the cells were incubated in 5 mM $CaCl_2$ for 15 min at 37℃ in the dark. The stained cells were analyzed with a FACSCalibur flow cytometer (Becton Dickinson) and Cell Quest software (Becton Dickinson) at the same laboratory. The fluorescence of AV and that of PI were measured through 550 nm and 690 nm filters, respectively, after 488 nm fluorescence emission. The ratio of positive cells was determined by the evaluation criteria using negative and positive controls. The particles were analyzed by measuring their relative diameter using the degree of forward scatter. We defined particles smaller than normal cells as microparticles. The percentage of microparticles among total particles (1,000 particles) was calculated. For particle analysis, 10 μL cell pellets in bio-phantoms were taken from the upper and lower parts of the bio-phantoms and were diluted by 10 mL of PBS in order to calculate the precise mean percentage of microparticles for each bio-phantom. These analyses were performed using Summit software (Becton Dickinson).

DW MR imaging.   The phantoms were placed into a phantom container (Fig. 1D), which was filled with PBS and then heated to 37℃ using a water bath. The container and a heat-retention gel material were put into a homemade case of styrene foam to keep the phantom temperature at 36.5 ± 0.5℃ during MR imaging. MR images of the container were taken by a head coil with a 1.5-tesla MRI device (Achieva, Philips Electronics Japan, Tokyo, Japan) as shown in Fig. 1E. Triaxial DW images were taken orthogonally with motion-probing gradients applied in the x, y, z directions by a multi-shot echo planar imaging sequence. The number of shots was set to 9. The scan parameters were set as follows: repetition time = 2000 ms; echo time = 100 ms; field of view (FOV) = 100 × 100 mm; matrix = 256 × 256; b values = 0, 250, and 500 s/mm²; thickness = 5 mm; the time interval between the onset of diffusion-gradient pulses (Δ) = 30.0 ms; the diffusion gradient pulse duration (δ) = 17.4 ms; the effective diffusion time ($\Delta-\delta/3$) = 24.2 ms; and the diffusion gradient pulse (G) = 0 to 30.9 mT/m.

Calculation of ADC values.   The isotropic DW image for each b value was created from triaxial DW images by calculating the root-mean-square of the logarithms of signals at each pixel. The ADC value was determined for each pixel on isotropic DW images

by calculating the change rates of the signals of isotropic DW images against the b values using the least-squares methods. The ADC map was made using the ADC value of each pixel on the isotropic DW images (Fig. 1F). The ADC values of the bio-phantoms were calculated from the square region of interest on the ADC map using Image-J software.

Results

ADCs of normal cells and sonicated cells. The ADC values of normal cells decreased as cell density increased (Fig. 2A). The destruction of the cell membranes by sonication increased the ADC values compared with normal cells, and the ADC values decreased linearly according to the increase in cell density (Fig. 2A). The ADC values of bio-phantoms were reduced according to the decrease in the center-to-center distance of cells (Fig. 2B). When the cell density was within the range between 3.0×10^7/mL and 4.5×10^8/mL, a range in which the center-to-center distance between cells was large, the ADC values of normal cells were reduced linearly according to the increase in cell density. When the cell density increased in the range between 5.5×10^8/mL and 1.3×10^9/mL, the range in which the center-to-center distance decreased to less than 15 μm, the ADC values of normal cells declined steeply and with a sweeping form. The reduction rate of the ADC values of sonicated cells as a function of cell density was -4.84×10^{-13} mL mm²/s, which was about one third of that for normal cells, -1.39×10^{-12} mL mm²/s (Fig. 2A).

Morphological observations of cells.   Cell size and shape were studied from light microscope images (Fig. 3A, B), and the diameter of Ramos cells was determined to be 11.6 ± 1.1 μm. Sonication destroyed the membrane structures, including the cell membranes, and normal cells did not remain (Fig. 3C). The SEM observation revealed increased numbers of rituximab-treated cells in budding (Fig. 3E) on the cell surfaces as well as increased numbers of microparticles (Fig. 3F) as apoptotic bodies in the extracellular spaces compared to normal cells (Fig. 3D). The TEM observation also revealed budding on the surfaces of the rituximab-treated cells compared with normal cells (Fig. 3G). The budding bulged from the cell surface, and the density inside the budding was similar to that of the cytoplasm. The density
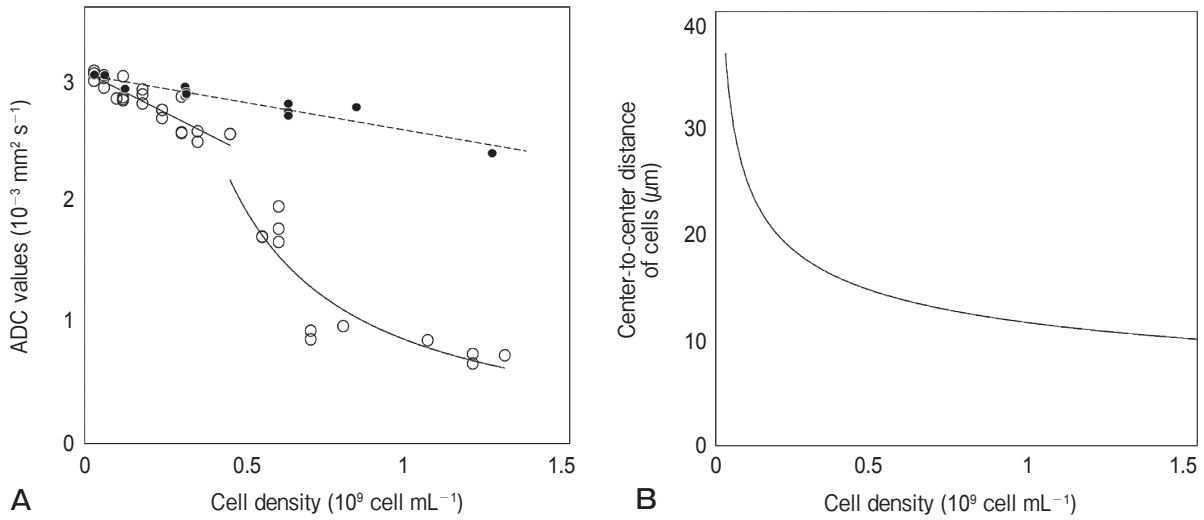
Fig. 2 ADC values of bio-phantoms including cells and the center-to-center distances between cells in bio-phantoms. (**A**) The relationships between ADC values and cell densities of bio-phantoms. The symbol (○) shows normal cells and the straight black line is the regression line obtained from the dates of cell density within the range between 3.0×10^7/mL and 4.5×10^8/mL. The symbol (●) shows sonicated cells and the dashed black line is the regression line. (**B**) The relationships between center-to-center distances and cell densities of bio-phantoms.
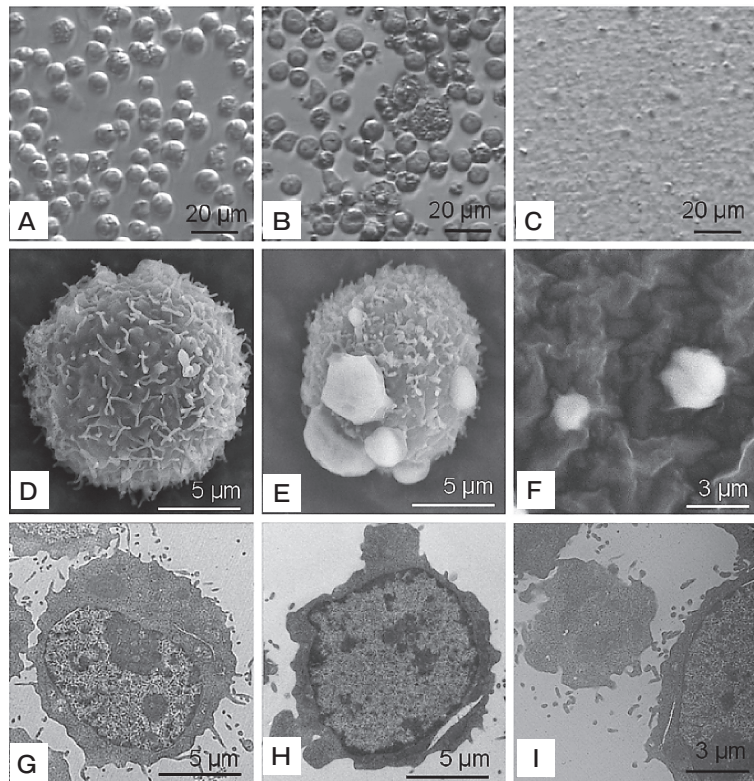

Fig. 3 The changes in cell morphology in response to sonication and rituximab treatment. (**A–C**) Light microscopic observation of cells. (**D–F**) Scanning electron microscopic observation of cells. (**G–I**) Transmission electron microscopic observation of cells. (**A**), (**D**), and (**G**) Normal cells. (**B**), (**E**), and (**H**) Apoptotic cells treated with rituximab. (**C**) Sonicated cells. (**F**) and (**I**) The microparticles appeared after rituximab treatment.

inside the microparticles (Fig. 3I) was also similar to that of the cytoplasm.

Flow cytometric analysis.   The flow cytometric analysis of the double staining with AV and PI showed a 7% increase in apoptotic cells in the early stage after rituximab treatment, as indicated by staining with AV alone and not by PI. Cells stained by both AV and PI increased 18%. Microparticle analysis revealed that a larger number of microparticles existed in bio-phantoms after rituximab treatment compared to the number in the bio-phantoms of normal cells (Fig. 4).

ADC of apoptotic cells.   After the cells were treated with rituximab, the cell density of the spinner flask was between $0.7 - 1.1 \times 10^6$/mL. The cells were centrifuged into cell pellets, and the maximum cell density was $4.0 - 4.5 \times 10^8$/mL (Table 1), whereas the maximum density of normal cells was $1.1 - 1.3 \times 10^9$/

mL. After centrifugation in the bio-phantom, the ADC value of the bio-phantom without gellan gum was $0.91 \pm 0.06 \times 10^{-3}$mm^2/s (Table 1), which was significantly lower than that of normal cells (Fig. 2A), the density of which was the same as that of treated cells.

Discussion

We measured the ADC values of bio-phantoms in which gellan gum was used to change cell density and distribute cells with uniform extracellular spaces. In a previous *in vitro* study [24], extracellular spaces were not uniform and could not be clalculated exactly, because swelling and shrinking cells had varying radii. In other *in vitro* studies [25, **26**], the precise extracellular spaces were also not calculated. In most of these *in vitro* reports, the ADC measurements were not done at a physiological temperature, 37℃. Under these experimental conditions, the obtained ADC values might be low compared to those in clinical situations, in which cells exist at about 37℃. The ADC measurements at low temperature might make it difficult to distinguish between the free diffusion at extracellular space and the restricted diffusion at intracellular space using low b values.

The ADC values of bio-phantoms were closely related to the cell density. The ADC values of normal cells were determined simply by cell density and were not influenced by the amount of extracellular space when the cell density was within the range between 3.0×10^7/mL and 4.5×10^8/mL. When the cell density increased to between 5.5×10^8/mL and 1.3×10^9/mL, the range in which the distance between cells became less than 4μm, the ADC values decreased remarkably because the average diameter of Ramos cells was 11.6μm. We consider that the restriction of water diffusion at the extracellular space significantly affected the ADC values of bio-phantoms in this narrow extracellular space of less than 4μm. In previous reports [8, 9, 15] of the measurement of *in vivo* ADC values and in the comparison between the ADC values and histological findings, it was difficult to determine that the decrease in ADC values was due simply to the increase in cell density and to evaluate the degree to which the amount of extracellular space affected these values.

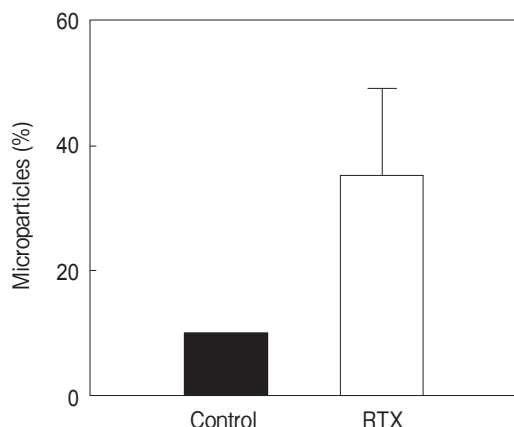Our study clarified that the destruction of the cell membrane by sonication increased ADC values.

Fig. 4   The rate of microparticle appearance rate. The vertical axis indicates the percentage of microparticles in bio-phantoms. The control is the percentage in the bio-phantom of normal cells. RTX is the percentage in the bio-phantom of cells treated by rituximab.

Table 1   ADC values and cell density of bio-phantoms treated by rituximab

Phantom	ADC ($\times 10^{-3}$mm^2/s)	Cell density ($\times 10^9$/mL)
# 1	0.96	0.44
# 2	0.95	0.40
# 3	0.90	0.42
# 4	0.83	0.45
Mean ± standard deviation	0.91 ± 0.06	0.43 ± 0.02

Several *in vivo* studies [8, 12, 13] have clarified that the destruction of the cell membrane, which acts as a barrier against the diffusion of water molecules increases the ADC values of cells through necrosis. The ADC values of sonicated cells decreased linearly with the increase in cell density even in the range of high cell density. This means that sonication eliminated the restriction of water diffusion due to intracellular membrane structures and narrow extracellular spaces. The decrease in ADC values in normal cells was a result of the presence of intracellular components and structures. On the other hand, the decrease in those values in sonicated cells was yielded by intracellular components alone, because of the destruction of cell membranes. The slopes of the decreases in the ADC values of normal cells and sonicated cells were in the ratio of 1 to 0.35. It suggests that approximately 65% of the ADC values of cells originated from the cell membrane structure and 35% originated from intracellular components.

Rituximab is a molecularly targeted drug and anti-CD20 antibody that induces apoptosis [20, 21]. When apoptosis occurred, budding on the cell surfaces and microparticles in the extracellular spaces among cells appeared and the maximum cell density of the bio-phantom decreased. The ADC values of the bio-phantoms including apoptotic cells were significantly decreased compared to those of normal cells, which had a cell density identical to that of apoptotic cells. This suggests that microparticles enter the extracellular spaces and might restrict the water diffusion therein. This *in vitro* report revealed that apoptotic bodies might play an important role as barriers against water diffusion in extracellular spaces. Wendland *et al.* [27] reported that apoptosis occurred due to the hypoxic injury of brain tissues and was decreased in *in vivo* ADC values, although the mechanisms underlying these actions were not identified. This decrease in ADC values during apoptosis might be caused by the blocking of water diffusion into the extracellular spaces by apoptotic bodies. On the other hand, some reports [17–19] have indicated that the *in vivo* ADC values of tumors increased when apoptosis occurred. Those reports suggested that cell shrinkage and a decrease in cell density were the mechanisms by which ADC values increased during apoptosis. Apoptotic cells usually appear in part of the tissue *in vivo*. Then shrinkage and budding occur and the cells are removed by phagocytes. The *in vitro* apoptotic process observed in the present study might not be identical to the *in vivo* apoptotic process. Therefore, our results might have a limited ability to explain the entire mechanisms of the alteration of ADC values during apoptosis in the clinic.

Various factors [8–19] are known to affect intricately the *in vivo* ADC values of tissues. Our methods, using bio-phantoms made of gellan gum, could make it possible to examine each individual effect of these factors, such as intracellular components, membrane structures, cell density, and extracellular space, on the change in ADC values. In our bio-phantom study, ADC values decreased according as cell density increased and, when the extracellular space became less than 4μm, the ADC values decreased suddenly by restricted diffusion. The bio-phantom allows us to analyze the impact of extracellular spaces on ADC values. We compared normal cells with sonicated cells and clarified the ratio of cell membrane structure to intracellular components for creating ADC values. Finally, microparticles from apoptotic cells migrated to the extracellular space and restricted the water diffusibility. To explain the complete mechanisms underlying the alteration of *in vivo* ADC values in tumor tissues, we should continue to analyze other factors that affect ADC values separately, as well as to interpret their impact in combination.

References

1. Padhani AR, Liu G, Koh DM, Chenevert TL, Thoeny HC, Takahara T, Dzik-Jurasz A, Ross BD, Van Cauteren M, Collins D, Hammoud DA, Rustin GJ, Taouli B and Choyke PL: Diffusion-weighted magnetic resonance imaging as a cancer biomarker: Consensus and recommendations. Neoplasia (2009) 11: 102–125.
2. Tsushima Y, Takahashi-Taketomi A and Endo K: Magnetic resonance (MR) differential diagnosis of breast tumors using apparent diffusion coefficient (ADC) on 1.5-T. J Magn Reson Imaging (2009) 30: 249–255.
3. Kloska SP, Wintermark M, Engelhorn T and Fiebach JB: Acute

stroke magnetic resonance imaging: Current status and future perspective. Neuroradiology (2010) 52: 189–201.

4. Sehy JV, Ackerman JJH and Neil JJ: Apparent diffusion of water, ions, and small molecules in the *Xenopus oocyte* is consistent with Brownian displacement. Magn Reson Med (2002) 48: 42–51.

5. Nicoli F, Lefur Y, Denis B, Ranjeva JP, Confort-Gouny S and Cozzone PJ: Metabolic counterpart of decreased apparent diffusion coefficient during hyperacute ischemic stroke-A brain proton magnetic resonance spectroscopic imaging study. Stroke (2003) 34: E82–E87.

6. Matsumoto Y, Kuroda M, Matsuya R, Kato H, Shibuya K, Oita M, Kawabe A, Matsuzaki H, Asaumi J, Murakami J, Katashima K, Ashida M, Sasaki T, Sei T, Kanazawa S, Mimura S, Oono S, Kitayama T, Tahara S and Inamura K: *In vitro* experimental study of the relationship between the apparent diffusion coefficient and changes in cellularity and cell morphology. Oncol Rep (2009) 22: 641–648.

7. Oliveira JT, Martins L, Picciochi R, Malafaya IB, Sousa RA, Neves NM, Mano JF and Reis RL: Gellan gum: A new biomaterial for cartilage tissue engineering applications. J Biomed Mater Res A (2010) 93A: 852–863.

8. Lyng H, Haraldseth O and Rofstad EK: Measurement of cell density and necrotic fraction in human melanoma xenografts by diffusion weighted magnetic resonance imaging. Magn Reson Med (2000) 43: 828–836.

9. Gibbs P, Liney GP, Pickles MD, Zelhof B, Rodrigues G and Turnbull LW: Correlation of ADC and T2 measurements with cell density in prostate cancer at 3.0 Tesla. Invest Radiol (2009) 44: 572–576.

10. Stadnik TW, Chaskis C, Michotte A, Shabana WM, van Rompaey K, Luypaert R, Budinsky L, Jellus V and Osteaux M: Diffusion-weighted MR imaging of intracerebral masses: Comparison with conventional MR imaging and histologic findings. Am J Neuroradiol (2001) 22: 969–976.

11. Guo AC, Cummings TJ, Dash RC and Provenzale JM : Lymphomas and high-grade astrocytomas: Comparison of water diffusibility and histologic characteristics. Radiology (2002) 224: 177–183.

12. Kamel IR, Bluemke DA, Ramsey D, Abusedera M, Torbenson M, Eng J, Szarf G and Geschwind JF: Role of diffusion-weighted imaging in estimating tumor necrosis after chemoembolization of hepatocellular carcinoma. Am J Neuroradiol (2003) 181: 708–710.

13. Lang P, Wendland MF, Saeed M, Gindele A, Rosenau W, Mathur A, Gooding CA and Genant HK: Osteogenic sarcoma: Noninvasive *in vivo* assessment of tumor necrosis with diffusion-weighted MR imaging. Radiology (1998) 206: 227–235.

14. Thoeny HC, De Keyzer F, Chen F, Ni YC, Landuyt W, Verbeken EK, Bosmans H, Marchal G and Hermans R: Diffusion-weighted MR imaging in monitoring the effect of a vascular targeting agent on rhabdomyosarcoma in rats. Radiology (2005) 234: 756–764.

15. Humphries PD, Sebire NJ, Siegel MJ and Olsen OE: Tumors in pediatric patients at diffusion-weighted MR imaging: Apparent diffusion coefficient and tumor cellularity. Radiology (2007) 245: 848–854.

16. Kilickesmez O, Yirik G, Bayramoglu S, Cimilli T and Aydin S: Non-breath-hold high b-value diffusion-weighted MRI with parallel imaging technique: apparent diffusion coefficient determination in normal abdominal organs. Diagn Interv Radiol (2008) 14: 83–87.

17. Morse DL, Galons JP, Payne CM, Jennings DL, Day S, Xia GW and Gillies RJ: MRI-measured water mobility increases in response to chemotherapy via multiple cell-death mechanisms. NMR Biomed (2007) 20: 602–614.

18. Huang MQ, Pickup S, Nelson DS, Qiao H, Xu HN, Li LZ, Zhou R, Delikatny EJ, Poptani H and Glickson JD: Monitoring response to chemotherapy of non-Hodgkin's lymphoma xenografts by T2-weighted and diffusion-weighted MRI. NMR Biomed (2008) 21: 1021–1029.

19. Kim H, Morgan DE, Buchsbaum DJ, Zeng HD, Grizzle WE, Warram JM, Stockard CR, McNally LR, Long JW, Sellers JC, Forero A and Zinn KR: Early therapy evaluation of combined anti-death receptor 5 antibody and gemcitabine in orthotopic pancreatic tumor xenografts by diffusion-weighted magnetic resonance imaging. Cancer Res (2008) 68: 8369–8376.

20. Zhou XH, Hu WG and Qin XB: The role of complement in the mechanism of action of rituximab for B-cell lymphoma: Implications for therapy. Oncologist (2008) 13: 954–966.

21. Flavell DJ, Warnes SL, Bryson CJ, Field SA, Noss AL, Packham G and Flavell SU: The anti-CD20 antibody rituximab augments the immunospecific therapeutic effectiveness of an anti-CD19 immunotoxin directed against human B-cell lymphoma. Br J Haematol (2006) 134: 157–170.

22. Hales TC: A proof of the Kepler conjecture. Annals of Mathematics (2005) 162: 1065–1185.

23. Honda O, Kuroda M, Joja I, Asaumi J, Takeda Y, Akaki S, Togami I, Kanazawa S, Kawasaki S and Hiraki Y: Assessment of secondary necrosis of Jurkat cells using a new microscopic system and double staining method with annexin V and propidium iodide. Int J Oncol (2000) 16: 283–288.

24. Anderson AW, Xie J, Pizzonia J, Bronen RA, Spencer DD and Gore JC: Effects of cell volume fraction changes on apparent diffusion in human cells. Magn Reson Imaging (2000) 18: 689–695.

25. Roth Y, Ocherashvilli A, Daniels D, Ruiz-Cabello J, Maier SE, Orenstein A and Mardor Y: Quantification of water compartmentation in cell suspensions by diffusion-weighted and T2-weighted MRI. Magn Reson Imaging (2008) 26: 88–102.

26. Pilatus U, Shim H, Artemov D, Davis D, vanZijl PCM and Glickson JD: Intracellular volume and apparent diffusion constants of perfused cancer cell cultures, as measured by NMR. Magn Reson Med (1997) 37: 825–832.

27. Wendland MF, Faustino J, West T, Manabat C, Holtzman DM and Vexler ZS: Early diffusion-weighted MRI as a predictor of caspase-3 activation after hypoxic-ischemic insult in neonatal rodents. Stroke (2008) 39: 1862–1868.